Mechanical Characterization of Toughened Polyamide-6 Blends with Metallocene Copolymers

S. López-Quintana,[1] C. Rosales,[2] I. Gobernado-Mitre,[1] J. C. Merino,[1,3] J. M. Pastor[1,3]

[1]*CIDAUT, Foundation for Research and Development in Transport and Energy, Parque Tecnológico de Boecillo, 47151 Boecillo, Valladolid, Spain*
[2]*Dpto. de Mecánica. Universidad Simón Bolívar, Apdo 89000, Caracas 1081, Venezuela*
[3]*Departmento de Física de la Materia Condensada E.T.S.I.I. Universidad de Valladolid, Paseo del Cauce s/n. 47011, Valladolid, Spain*

Received 2 March 2007; accepted 30 September 2007
DOI 10.1002/app.27459
Published online 26 November 2007 in Wiley InterScience (www.interscience.wiley.com).

ABSTRACT: The effectiveness as impact modifier of two *in situ* maleated metallocene copolymers, a metallocene polyethylene, (mPE1) and a metallocene ethylene-propylene (mEPDM) and three commercial maleated copolymers (mPE2-*g*-MA, EPDM-*g*-MA, and mEPR-*g*-MA) were studied in binary and ternary blends carried out in an intermeshing corotating twin-screw extruder with polyamide-6 (PA) as matrix (80 wt %). Also, the effects of the grafting degree, viscosity ratio, and crystallinity of the dispersed phases on the morphological and mechanical properties of the blends were investigated. A significant improvement of the compatibility of these grafted copolymers with PA6 was shown by FTIR spectroscopy, capillary rheometry, and scanning electron microscopy (SEM) in all reactive blends. The tensile strength values of the mEPR-*g*-MA/PA2 binary blend showed the highest strain hardening. The results obtained in this work indicated that the effectiveness of the grafted copolymers as impact modifier depends on the morphology of the blends and a combination of tensile properties of the blend components such as Young's modulus, Poisson ratio, and break stress. © 2007 Wiley Periodicals, Inc. J Appl Polym Sci 107: 3099–3110, 2008

Key words: toughening; polyamide-6; metallocene copolymers; blends; impact strength

INTRODUCTION

Many semicrystalline engineering polymers including polyamides, isotactic polypropylene, and linear polyethylene exhibit high strength and ductility at room temperature and under moderate rates of deformation. However, they become brittle under notching conditions and can undergo a sharp ductile-to-brittle transition. In the brittle regime, a crack can propagate with little resistance. Because of this poor performance at extreme conditions, there has been considerable commercial and scientific interest in the toughening of semicrystalline engineering thermoplastic materials.[1] Toughening of the semicrystalline polymers with rubber particles has been extensively studied over the last two decades. Rubber-modified polyamides have been extensively studied to obtain new materials with high-notched Izod impact properties at room and low temperatures.[2–7] Metallocene polyethylenes have been more studied as toughers than the metallocene copolymers.[4–6] Also, there are several studies that have documented the effect of parameters such as rubber particle sizes, volume fraction and interparticle distance, rubber particles distribution, Young's modulus, Poisson ratio, and stress strength of the rubber on the effectiveness of toughening in PA6/rubber blends.[8–11]

On the other hand, the main shortcoming of the rubber-toughened blends is the significant reduction of Young's modulus, which is caused mainly by the addition of a rubber with a low Young's modulus, such as EPDM-*g*-MA and mEPR-*g*-MA.[4–7] It is well known that the mechanical properties of polymer blends are strongly influenced by their morphology. In immiscible polymer blends, the morphology achieved depends, in general, on the blend composition, interfacial tension between the components, viscosity ratio, melt elasticity of the components, and processing history.[12,13] It is now well established that the phase morphology of immiscible polymer blends can be controlled by addition or *in situ* formation of compatibilizers, which can act as interfacial agents.[1,14]

For many common applications, PA6 is a tough polymer and does not need further toughening. However, there are numerous specific applications

Correspondence to: C. Rosales (crosales@usb.ve).
Contract grant sponsor: CYTED Program (Proyect VIII.11).
Contract grant sponsor: Ministerio de Educación de Ciencia; contract grant number: MAT2005-06627-003.

TABLE I
Characteristics of the Neat Polymers

Material	Commercial designation	ρ (g/cm^3)	MFI (°/min) or Mooney viscosity[a]	Ethylene content (wt %)
PA1	Akulon K 222D	1.14	40	–
PA2	Radilon S40 EN	1.14	3.6	–
mPE1	Engage 8402	0.90	30	–
mPE2-*g*-MA	Fusabond MN 493D	0.87	1.3	–
mEPDM	Nordel IP 3722P	0.88	19[a]	71
EPDM-*g*-MA	Royaltuf 485B	0.85	30[a]	75
mEPR-*g*-MA	Exxelor VA1801	0.87	9[b]	43

[a] MFI (dg/min).
[b] Determined at 10 kg of load and 230°C.

under notching conditions for which its toughness needs to be substantially increased. The goal of this work is to provide an evaluation on the effectiveness as toughening material of grafted metallocene copolymers with low crystallinity degrees, in binary and ternary blends with PA6, which have been analyzed in terms of capillary rheometry, FTIR spectroscopy, SEM morphology, tensile properties, and notched Izod impact behavior at room temperature and −30°C of temperature.

EXPERIMENTAL

Materials

Several types of commercial metallocene elastomers: a metallocene polyethylene (mPE1) and a metallocene ethylene-propylene diene copolymer (mEPDM) and two polyamides-6 (coded as PA1 and PA2) with different molecular weights were used as dispersed and continuous phase in the blends, respectively (Table I). On the other hand, different maleic anhydride modified random ethylene copolymer rubber was employed as compatibilizers: a metallocene polyethylene (mPE2-*g*-MA), a metallocene ethylene–propylene copolymer (mEPR-*g*-MA), and an ethylene–propylene diene copolymer (EPDM-*g*-MA). In some cases, the melt grafting of maleic anhydride (MA) onto mPE1 and mEPDM was *in situ* carried out by reactive extrusion according to the method described elsewhere.[15–17]

Melt processing

The blending and grafting processing were carried out in an intermeshing corotating twin-screw extruder (Leistritz 27 GL) at different processing conditions (extrusion speed and MA/peroxide ratio; Table II). The dispersed phases of the reactive blends, named B2 and B5 (Table II), were *in situ* maleated attending to the optimal grafting conditions already studied in a previous work.[16] Nonreactive and reactive (with grafted materials as dispersed phases and/or compatibilizers) binary and ternary PA6 blends were prepared with a constant PA6 concentration (80 wt %).

The barrel temperature profile was set between 150 and 240°C. The screw speed and another extrusion conditions employed for the grafting and blending are showed in Table II. An antioxidant Irganox B1171 (blend 1 : 1 of Irganox 1098 and Irgafos 168) was used (0.2 wt %) to prepare two PA6 masterbatches (PA1-AMB and PA2-AMB), which was added at the first port of the extruder. The dispersed phase was added at the second one. The test specimens for determining the mechanical properties were prepared by injection molding at 230°C in an injection-molding machine (Margarit JSW, JM 110). The polyamides and their blends were dried at 80°C for 24 h before blending and testing.

IR spectroscopic analysis

The FTIR spectra of the functionalized polymers and blends were obtained using the ATR technique

TABLE II
Extrusion Conditions for Grafting and Blending, and Designation of Blends

Process and/or blend	*T* (°C)	R.P.M	Mass flow rate (kg/h)
mEPDM and mPE1 grafting (1)	120	100	6.0
mEPDM grafting (2)	120	100	6.0
mPE1 grafting (2)	190	60	3.0
Masterbaches of PAs with antioxidants (PA1-AMB and PA2-AMB)	230	60	7.0
mPE1/PA1 (B1)	240	120	7.0
mPE1-*g*-MA/PA1 (B2)	240	85	6.0
mPE2-*g*-MA/PA1 (B3)	240	100	6.0
mEPDM/PA2 (B4)	240	80	3.0
mEPDM-*g*-MA/PA2 (B5)	240	85	6.0
mEPR-*g*-MA/PA2 (B6)	240	80	3.0
EPDM-*g*-MA/PA2 (B7)	240	80	3.0
mEPDM/PA2/EPDM-*g*-MA (B8)	240	80	3.0
mEPDM/PA2/mEPR-*g*-MA (B9)	240	80	3.0

(Golden Gate Diamant ATR) on a MB155 BOMEM FTIR spectrometer. Samples prepared as thick pressed melt films were analyzed in the range 4000–500 cm^{-1} at a resolution of 2 cm^{-1} and 32 scans/spectrum. All spectra are baseline corrected and shown as absorbance like ATR units. Grafting efficiency of maleic anhydride (MA) on elastomers was evaluated with the IR band responsible for stretching vibrations of a C=O bond in MA situated at a wavenumber 1780–1790 cm^{-1} and the C—H bending vibrations in $—CH_2$ groups in mPE1 at 720 cm^{-1}.[18,19] For mEPDM, the bands between 1830–1750 and 1750–1660 cm^{-1} were analyzed, and the band in the region of 760–680 cm^{-1} was used as internal standard.[16] The residual monomer was eliminated by dissolution in *ortho*-dichlorobencene at 120°C before the characterization of the grafted products.

Also, the influence of the compatibilizer on the copolymer formation was evaluated on the B3, B5, and B7 blends. The samples preparation consisted on a selective extraction by using formic acid and hot xylene as solvents. The soluble and insoluble fractions were separated, and the residues (isolated copolymer from as B3, B5, and B7) were dried and analyzed. This selected extraction was also applied for all blends like a solubility test (Molau test).[20–22]

Rheometry, thermal properties, and morphology

Capillary rheological measurements of the neat polymers and their blends were performed on a Göttfert Reograph 2002 capillary rheometer with an L/D ratio of 30 : 1 at 240°C. The examinated shear rates varied between 10 and 1000 s^{-1}. The PAs and their blends were dried before each testing. The melting and crystallization behavior of the neat and grafted polymers was studied by differential scanning calorimetry (DSC) by using a Mettler Toledo DSC 821/400, under nitrogen blanket at cooling and heating rates of 20°C/min. Morphological studies were conducted by scanning electron microscopic (SEM) analysis using a Jeol-820 scanning electron microscope. Cryogenically fractured etched specimens were used for morphological analysis. For each blend, different micrographs were made and analyzed after gold coating and an accelerating voltage of 20 kV. In some blends etching by *o*-xylene to remove the elastomer (or elastomer-*g*-MA) selectively was needed.

Mechanical properties and vicat temperature

The values of the mechanical parameters determined from both tensile and impact tests reflect an average from at least five measurements. The tensile tests were carried out using an Instron 2525-806 tensile tester at a cross-head speed of 1 and 10 mm/min at room temperature according to UNE-EN ISO 527, 1 and 2 standard method. The mechanical properties (Young's modulus, tensile strength, and ductility measured as the break strain) were determined from the load-displacement curves. Izod impact tests were carried out on notched specimen, according to UNE-EN-ISO 180/1 at two temperatures 23°C and −30°C, using a CEAST 6548/000 pendulum. The notch (depth 2.54 mm and radius 0.25 mm) was machined after injection molding. A minimum of 10 impact specimens were tested for each reported value. Also, impact puncture test were performed for some blends, following ISO 6603-2:2000 at 23°C. The Vicat temperatures were obtained by an A/3M ATS-Faar HDT-Vicat tester at 120°C/h of heating rate.

RESULTS AND DISCUSSION

Grafting degree, viscosity ratio, and thermal behavior of the blend components

In reactive blends, grafted materials have to be used to increase the performance of the products.[1–7] The processing conditions and proportions of grafting agent (MA) and peroxides employed in the functionalization reactions of mPE1 and mEPDM materials were chosen to get the maximum grafting degree with the minimum secondary reactions.[15–19] ATR-FTIR spectra were obtained for the functionalized products to determine their grafting degrees. In the spectra of the functionalized products with MA, two bands were observed at 1780–1790 cm^{-1} and 1712 cm^{-1}. They can be associated to the stretching vibrations of the C=O bond in MA and to the same vibrations from the hydrolyzed groups of the maleic anhydride, which is partially converted to the acid form.

The band area ratios of 1785 cm^{-1}/1375 cm^{-1}, 1710 cm^{-1}/1375 cm^{-1} and the peak height ratios of 1785 cm^{-1}/720 cm^{-1} were calculated to eliminate the dependence of the carbonyl peak area (and/or height) on the film thickness and used to obtain the grafting degree of the mEPDM-*g*-MA and mPE1-*g*-MA samples.[17–19] To determine the grafting or functionalization degree in the grafted products, several calibration curves reported by Moad,[18] White et al.,[19] and Oostenbrink and Gaymans[17] were employed. The use of these curves allows to determine quantitatively the functionalization degree (expressed as inserted maleic anhydride in wt %) in a simpler and more rapid way than by means of any other method of analysis described in the literature. The grafting degrees of the materials are reported in Table III. The higher grafting degree obtained for the mPE1-*g*-MA than that of the mEPDM-*g*-MA is in agreement with the higher proportion of MA used in the grafting processes of this material (6 and 4 wt %, respectively).

TABLE III
Absorbance Ratios ($A_{1785\ cm^{-1}}/A_{1375\ cm^{-1}}$, $A_{1710\ cm^{-1}}/A_{1375\ cm^{-1}}$), Grafting Degree of Functionalized Materials, and Shear Viscosity (η) at 72 s^{-1} of Shear Rate

Material	$\frac{A_{1785\ cm^{-1}}}{A_{1375\ cm^{-1}}}$	$\frac{A_{1710\ cm^{-1}}}{A_{1375\ cm^{-1}}}$	Grafting degree (wt %)	η at 72 s^{-1} (Pa s)
mPE1	0.00	0.00	0.00	127
mPE1-*g*-MA	1.16 ± 0.04	0.45 ± 0.02	0.69[a] (0.66)[b]	652
mPE2-*g*-MA	–	1.21 ± 0.06	0.53[a] (0.50)[c]	970
mEPDM	0.00	0.00	0.00	1543
mEPDM-*g*-MA	0.65 ± 0.04	0.24 ± 0.03	0.40[a] (0.54)[d]	2927
EPDM-*g*-MA	0.00	0.40 ± 0.02	0.19[a] (0.25)[c]	2625
mEPR-*g*-MA	0.030 ± 0.004	1.20 ± 0.06	0.95[b] (1.00)[c]	2275

[a] By using a calibration curve reported by Moad.[18]
[b] By using a calibration curve reported by White et al.[19]
[c] As reported by the commercial producers.
[d] By using a calibration curve reported by Oostenbrink and Gaymars.[17]

As well, the commercial mEPR-*g*-MA and EPDM-*g*-MA products showed the highest and lowest grafting degree, respectively.

During the grafting reactions of MA, crosslinking and/or degradation reactions may appear, which may affect the blend components viscosity and consequently the blending processing conditions.[15–19] A crosslinking reaction, even in a small proportion, will greatly increase the melt viscosity, perturbing the correct blending. The crosslinking extension secondary reactions are quantitatively indicated by the amount of xylene-insoluble fractions or gel content. A gel content of 17 and 0 wt % were obtained for the *in situ* mEPDM-*g*-MA and mPE1-*g*-MA samples, respectively. This high value in gel content for the functionalized *in situ* mEPDM could be related to the presence of double bonds in its structure. On the other hand, capillary rheometry was used to characterize the neat and grafted polymers. The polymers viscosities decreased as the shear rate increased, indicating a pseudoplastic behavior. The lower shear thinning character and the viscosity values for PAs and mPE materials were in accordance with their molecular characteristics: the PA1 has a lower molecular weight than PA2 and the metallocene mPE sample has a narrow molecular weight distribution.[23] Also, the viscosity of these grafted material was higher than that of the neat mEPDM and mPE1 materials due to the crosslinking secondary reactions and/or long-chain branching formation, respectively. The shear viscosities at 72 s^{-1} of shear rate are presented in Table III. The highest enhancement of viscosity at 72 s^{-1} of shear rate was obtained for the mPE1-*g*-MA product.

On the other hand, the morphology of the blends can be affected by the viscosity ratio of the blend components and the blending processing conditions.[12,13] Then the viscosity ratio of the binary blend components [viscosity of the dispersed phase (η_d)/viscosity of the matrix (η_m)] at 240°C was calculated as a function of shear rate (Figs. 1 and 2) for all components in binary blends. This value decreased with increasing shear rate due to higher shear thinning behavior of the different dispersed phases comparing with the PA materials. The viscosity ratio values of the blend components for the reactive blends are higher than the nonreactive ones, at all shear rates evaluated. Also, the blend components of reactive binary blends with PA1 have viscosity ratios higher than 2 at 100 $s^{-1}$of shear rate (Fig. 1). As well, the blend components of reactive binary blends with PA2 have similar viscosity ratios at higher shear rates and they are slightly higher than one at the average shear rate (80–100 s^{-1}) in the extruder (Fig. 2).

Also, the crystallization and melting behavior of the neat polymers were characteristic of these materials. In fact, a very broad crystallization exotherms

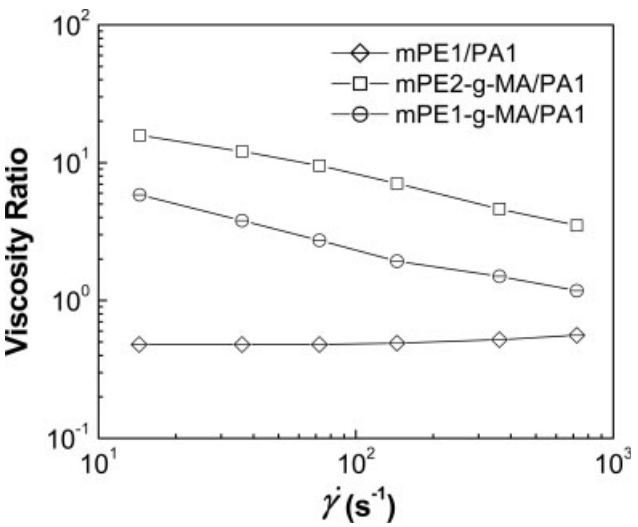

Figure 1 Viscosity ratio as a function of shear rate of the PA1 blends components at 240°C.

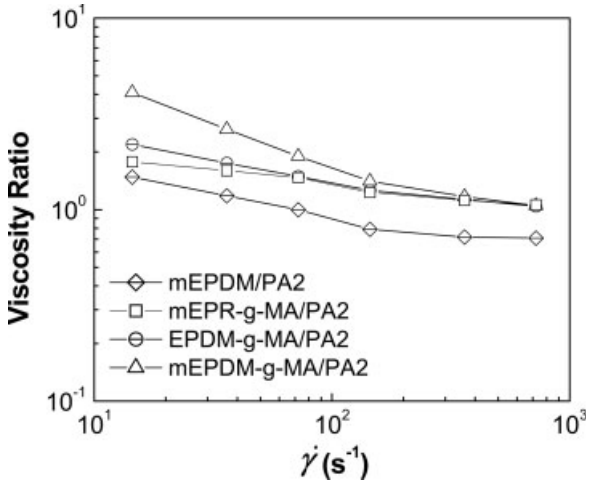

Figure 2 Viscosity ratio as a function of shear rate of the PA2 blends components at 240°C.

and melting endotherms for the PE copolymers samples (mPE1, mPE1-*g*-MA, mPE2-*g*-MA, mEPDM, mEPDM-*g*-MA, and mEPR-*g*-MA) can be obtained due to the higher ethylene content in the metallocene copolymers than that of other types of EPR rubbers.[24] However, two melting endotherms were found for the EPDM-*g*-MA. It can be assumed that the high temperature endotherm is related to the melting of a crystallizable material characterized by long methylene sequences having a low number of chain defects. More disordered or shorter polyethylene segments give rise to the broad low temperature endotherm, which falls below room temperature. Similar results were found by Greco et al.[25] in a grafted EPR with diethyl maleate. The thermal parameters of the neat and grafted copolymers are presented in Table IV. The values of the peak temperatures, crystallization (Tc_p), melting temperatures (Tm_p), and crystallinity (C) were found in the cooling and second heating, respectively. When the grafted mPE1-*g*-MA and mEPDM-*g*-MA samples were compared with its neat materials (mPE1 and mEPDM), the crystallinity of the grafted materials were similar than that of its neat polymers due to the low grafting degree in both materials. As well, the mPE2-*g*-MA, mEPDM-*g*-MA, EPDM2-*g*-MA, and mEPR-*g*-MA commercial copolymers have lower degrees of crystallinity than that of mPE1-*g*-MA material.

Morphology of the blends

The cryofractured surfaces of the injection-molded impact specimens were observed by SEM (Figs. 3 and 4). The uncompatibilized blends (nonreactive) exhibited a very broad size distribution and the adhesion level between PA and ungrafted copolymer is poor due to the lack of compatibility.[1] The experimental diameter of the dispersed phases (D_{exp}) of the blends are presented in Table V. The different morphologies and the highest sizes obtained in the nonreactive blends (B1 and B4) could be explained taking into account the differences between the viscosity ratios (η_d/η_m) of their components and the high coaslescence of the particles in uncompatibilized blends[12,13] (Table V). In contrast, the *in situ* copolymer formed by the reaction between the amine end groups of the PA and the MA group in the grafted materials in the binary reactive blends acted as compatibilizer and produced a very fine dispersion in the blends.[1,4–7] Also, the particle sizes of the reactive blends with grafted copolymers were smaller than the uncompatibilized ones due to the emulsifying effect and reduction in coalescence in these blends.[12,13] This proves that the dispersion and the compatibility of the blends are improved. The higher size of the dispersed phase for the B3 than that for B2 reactive blends is in according with the higher viscosity ratio of the blend components (see Fig. 1 and Table V). On the other hand, the particle sizes of the binary reactive blends with PA2 (B5, B6, and B7 blends) as matrix were all similar and smaller than that made with PA1 (B2 and B3 blends)

TABLE IV
Thermal Properties of the Neat Copolymers and PAs

Material	Tm_p (°C) (±2)	C[a] (%)	Tc_p (°C) (±2)	Melting range (°C)
PA1	221	42	189	170–240
PA2	222	41	186	170–240
mPE1	100	33	80	10–110
mPE1-*g*-MA	100	30	80	10–110
mPE2-*g*-MA	55–58	17	24	−40–80
mEPDM	44–50	14	26–30	−20–70
mEPDM-*g*-MA	44–50	12	24	−20–70
EPDM-*g*-MA	38 and 110	10	–	−10–135
mEPR-*g*-MA	45–55	14	24–28	−20–110

[a] Crystallinity was calculated by using 293 and 190 J/g for 100% crystalline PE and PA-6, respectively.[26]

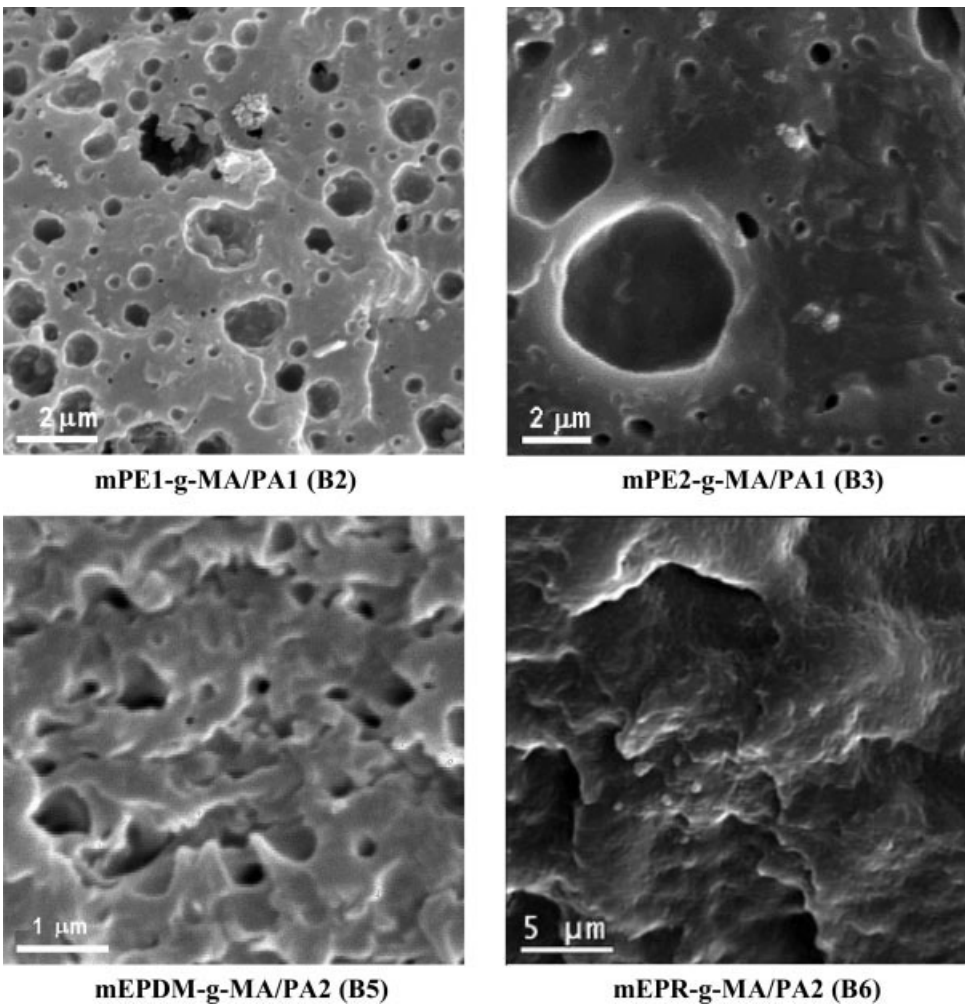

Figure 3 SEM morphology of the etched by xylene binary blends: mPE1-*g*-MA/PA1, mPE2-*g*-MA/PA1, and mEPDM-*g*-MA/PA2, and the binary blend: mEPR-*g*-MA/PA2.

due to their smaller viscosities ratios (see Fig. 2 and Table V).

The emulsifying effect of the compatibilizer in ternary blends (B8, B9, and B10) can be explained assuming that this material was mostly located at the interface of the dispersed phase/PA, acting as an interfacial agent.[14,27] In ternary blends, the dispersed phase particle size depends on the rheological properties of the components, matrix type, order of mixing, mixing intensity, extruder type, graft structure, maleation level of the compatibilizer, proportion, miscibility of dispersed phase and compatibilizer, and so on.[28–30] In the ternary blend preparations, the continuous phase (PA) and the minor component phase with compatibilizer were added at the feed and second port of the extruder, respectively. These modes of addition of the components were made to have a most homogeneous morphology.[14] Although, the mPE1 and mEPDM materials may not be miscible with the mEPR-*g*-MA sample, the similar and low dispersed phase particle sizes (Fig. 4 and Table V) found for the ternary blends made with mEPR-*g*-MA as compatibilizer (B9 and B10) could be due to the high grafting degree of the functionalized mEPR-*g*-MA (Table III). As well, the EPDM-*g*-MA has the lowest grafting degree.

Characterization of the blends by FTIR and capillary rheometry

To investigate the possible interactions between the blend components, the Molau test was applied.[20] A clear phase separation of the blend components was observed for the B1 nonreactive blend and a milky colloidal suspension was found for the B4 nonreactive and the reactive blends. This result obtained for the B4 blend may be due to physical interactions and/or mechanical grafting between PA2 and mEPDM sample. For the reactive blends, the chemical groups involved in possible reactions between PA and the grafted samples might originate new bands, which overlap the original components

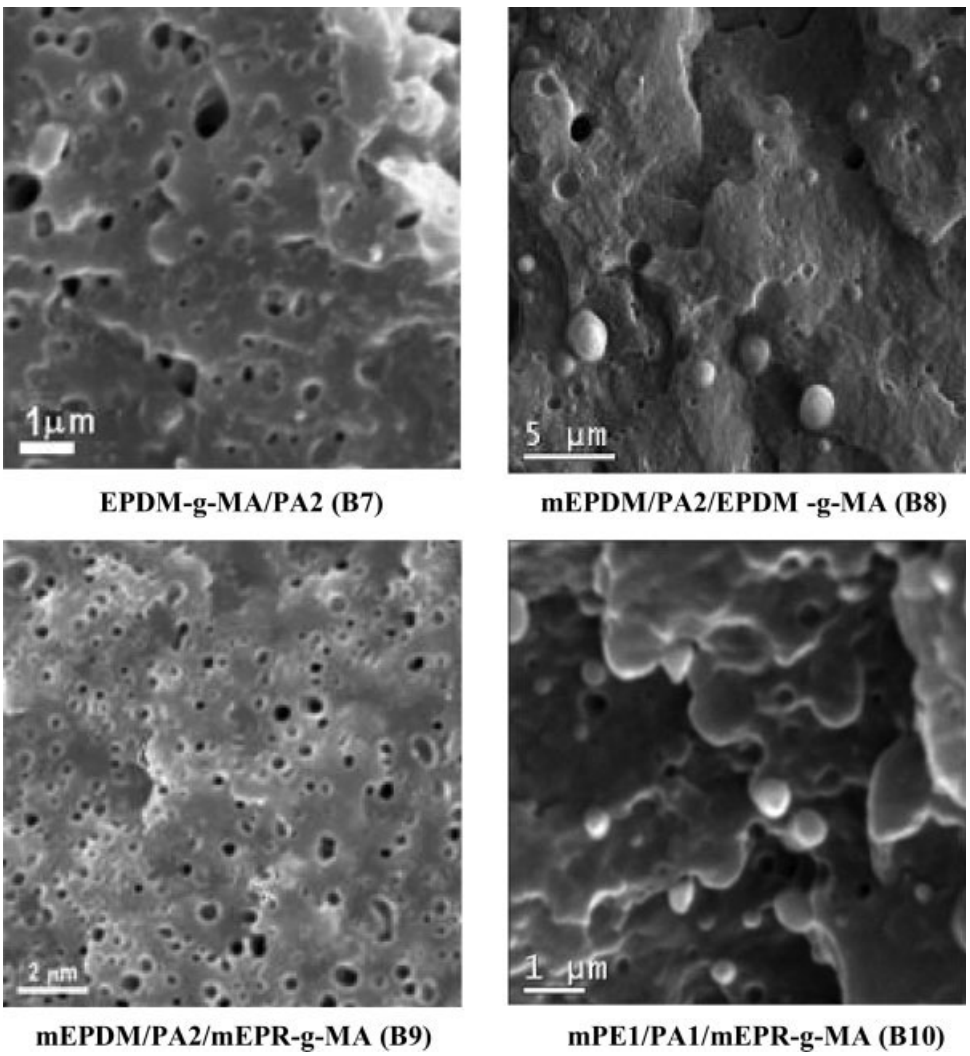

Figure 4 SEM morphology of the etched by xylene binary and ternary blends: EPDM-*g*-MA/PA2 and mEPDM/PA2/EPDM-*g*-MA, and the ternary blends: mEPDM/PA2/mEPR-*g*-MA and mPE1/PA1/mEPR-*g*-MA.

bands. Then, the infrared spectra obtained for the reactive and nonreactive blends were very similar. Additionally, the extent of chemical reaction and/or physical interactions might not be so large as to highly modify the spectra of reactive blends.[21,22] Once the formation of a copolymer was detected in the reactive blends, a selective extraction was conducted by the procedure early described in the experimental section for the B3, B5, and B7 blends. The resulting ATR-FTIR deconvoluted spectra, in the

TABLE V
Average Shear Rate in the Extruder, Viscosity Ratio (η_d/η_m), and Experimental Diameter (D_{exp}) and Interparticle Distance (τ) of the Dispersed Phases

Blend	Average shear rate (s^{-1})	η_d/η_m	D_{exp} (μm)	τ (μm)
mPE1/PA1 (B1)	120	0.48	5.0	–
mPE1-*g*-MA/PA1 (B2)	85	2.31	<1.5	<0.44
mPE2-*g*-MA/PA1 (B3)	100	3.61	<2.5	<0.88
mEPDM/PA2 (B4)	80	0.97	2.0	–
mEPDM-*g*-MA/PA2 (B5)	85	1.79	<1.0	<0.56
mEPR-*g*-MA/PA2 (B6)	80	1.45	<1.0	<0.56
EPDM-*g*-MA/PA2 (B7)	80	1.64	<0.7	<0.2
mEPDM/PA2/EPDM-*g*-MA (B8)	80	0.97	<2.0	<0.56
mEPDM/PA2/mEPR-*g*-MA (B9)	80	0.97	<0.8	<0.22
mPE1/PA1/mEPR-*g*-MA (B10)	100	0.48	<1.0	<0.28

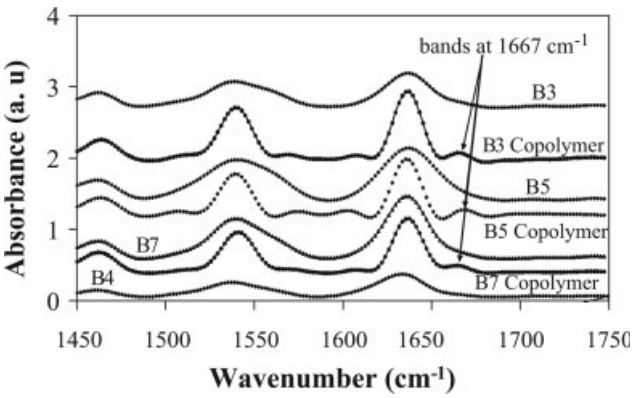

Figure 5 Deconvolution spectra for amides I and II regions in mEPDM/PA2 (B4), mEPDM-*g*-MA/PA2 (B5), EPDM-*g*-MA/PA2 (B7), and mPOE2-*g*-MA/PA1 (B3) blends and their copolymers.

amides I and II modes at 1636 and 1546 cm^{-1}, respectively, for the B3, B4, B5, and B7 blends, and their extracted copolymer (B3-COP, B5-COP, and B7-COP) are shown in Figure 5. The deconvolution of the spectra showed that the copolymers formed have more carbonyl groups because the band around 1667 cm^{-1} appears well defined with respect to those of the other blends. These results could be indicative of chemical interactions in reactive blends and/or chemical degradation of the PAs in the blend preparations.[21–22,31]

On the other hand, during steady shear flow, capillary rheometry was also used to characterize the extruded blends under relevant conditions before subsequent processing. The steady pressure readings observed for the extruded blends should correspond to a stabilized morphology, in which breakup and coalescence of the dispersed phase are balanced in nonreactive blends (B1 and B4). The viscosity curves as a function of the shear rate at 240°C of the blends with PA1 and PA2 as matrix are presented in Figures 6 and 7, respectively. The viscosity and shear thinning effect of PA2 are higher than PA1 because its high-average weight molecular weight (PA2 has a lower melt flow index value than PA1, Table I). The nonreactive binary blend with mEPDM1 as dispersed phase (B4) was less viscous than its continuous phase (PA2). On the other hand, an increase of the viscosity values was found for the reactive binary and ternary blends at low shear rates. Likewise, the shear thinning character of the blends was higher than that of its continuous phase component. This increase in viscosity and shear thinning behavior for the compatibilized blends could be due to an increase in interfacial adhesion as a result of *in situ* copolymer formation.[21,32,33]

Mechanical properties

It is well known that PA-6 has a pseudoductile behavior, a low-notched impact strength and a high-unnotched impact value.[34] The effect of compatibilizers on the notched Izod impact strength of the studied blends at two temperatures, 23°C and −30°C, is shown in Figures 8 and 9. All reactive blends showed stress-whitening after fracture. So, in the blends with low impact strength, the stress-whitening zone was only around the notch; meanwhile, super-tough PA blends showed an intense stress-whitening along the whole fracture surface. The impact strength values obtained in the binary nonreactive blends (B1 and B4) at room temperature are very low because the lack of adhesion between the phases. The notched Izod impact strength of PA-6 can be improved by blending with grafted rubbers.[1–7] The impact strength found in the binary blend (B5) prepared with the grafted *in situ*

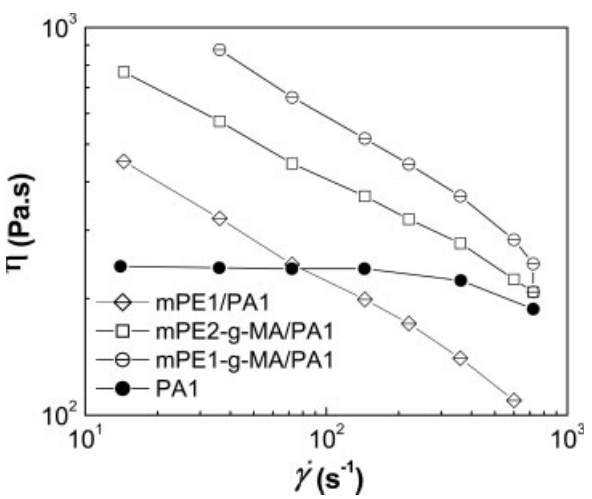

Figure 6 Viscosity as a function of shear rate of the blends with PA1 at 240°C.

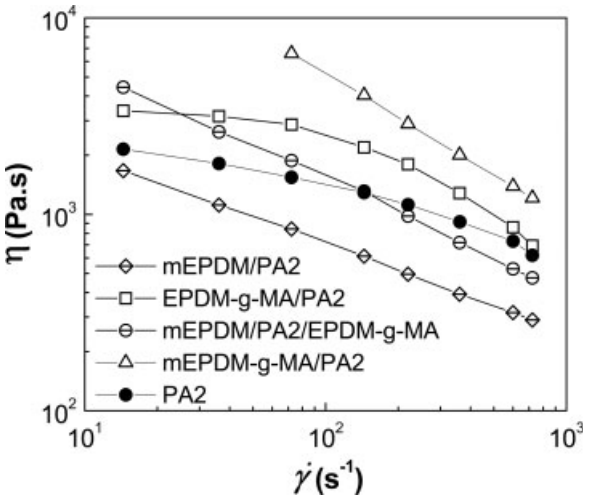

Figure 7 Viscosity as a function of shear rate of the blends with PA2 at 240°C.

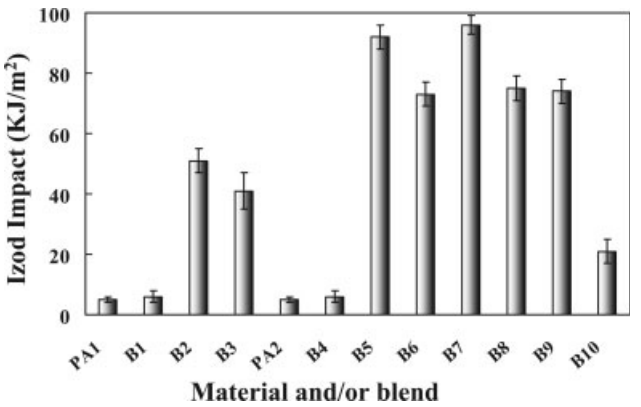

Figure 8 Notched Izod impact strength of the binary and ternary blends at room temperature.

mEPDM-*g*-MA sample was more than 17-fold that of neat PA2 and about 10-fold that of the corresponding nonreactive blend (B4). The compatibilizers EPR-*g*-MA and EPDM-*g*-MA employed in ternary blends seemed to behave qualitatively similarly in B8 and B9 blends; both grafted materials produced higher Izod impact strength at the two temperatures. Also, the notched Izod impact strength values of the corresponding binary blends (B6 and B7) were higher than those of ternary and nonreactive blends. The highest notched Izod impact strength was obtained for the B7 blend prepared with EPDM-*g*-MA with the lowest grafting degree (see Table III). This indicates that the relevant adhesion is not a unique condition for super-toughness in rubber binary toughened blends, and only low adhesion levels were enough to increase toughness.

On the other hand, the cavitations of isolated rubber particles and rubber interlayer represent the main mechanism of damage and volume dilatation for polymer blends. Because cavitations in PA particles were not encountered in blends with PA as dispersed phase, deformation damage is essentially controlled by rubber cavitations, interfacial debonding between the phases and matrix shear yielding.[35–37]

The requirements to achieve toughness in blends with a shear yield mechanism include (a) a range of rubber particle size and interparticle distance (τ), (b) uniform distribution of the rubber particles, (c) the components should be able to transfer the applied stress, (d) low modulus ratio between the rubber and the polyamide bulk phase, and (e) high Poisson's ratio with low breaking stress of the dispersed phase.[1,5–9,10,11] The (a), (b), and (c) requirements may be obtained by the control of the blend morphology and interactions between the components. Wu[38] proposed that the notched Izod impact strength increase should occur when the interparticle distance between two particles is below a critical value (τ_c). This value is characteristic of a given matrix, and it is independent of the rubber volume fraction and the particle size. The τ_c value found in blends with PA6 as matrix and grafted rubbers as dispersed phase is about 0.31 μm. In other blends with rubber dispersed phases, the critical interparticle distance to achieve toughness increases when the Young's modulus of the dispersed phase decreases.[10] On the other hand, the interparticle distance of the dispersed phase was calculated by the following equation:

$$\tau = d\left[(\pi/6\phi)^{1/3} - 1\right] \quad (1)$$

where τ is the interparticle distance, ϕ is the volume fraction of the dispersed phase, and d is the diameter of the dispersed phase.[1] The interparticle distance of the reactive blends calculated with this equation is shown in Table V. The notched Izod impact strength values obtained for the reactive binary blends cannot be explained either the interparticle distance or the Young's modulus values of the dispersed phases. The cavitations of isolated rubber particles and rubber interlayer represent the main mechanisms of damage and volume dilatation for polyamide-6 blends.

On the other hand, the other requirements may be achieved by selecting the blend components with high cavitations ability. The cavitations deformation values (ε_v) of the different dispersed phase materials were calculated by using the analysis of elastic-stress distribution in particle-dispersed blends developed by Liang et al.[11] In this analysis, the constituents are perfectly bonded together at the interface. The Young's modulus (E), Poisson's modulus (μ), and tensile strength (σ) of the matrix and dispersed phases employed for the binary blends preparation and employed in the Liang model are presented in Table VI. The cavitations deformations values (ε_v) calculated with this model as a function of Young's modulus of the dispersed phase (E_d) with two tensile

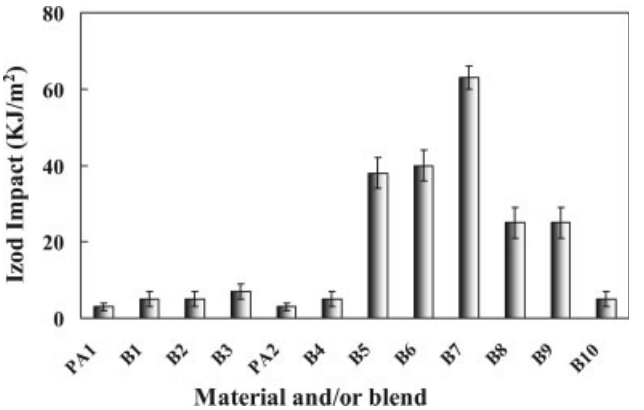

Figure 9 Notched Izod impact strength of the binary and ternary blends at −30°C of temperature.

TABLE VI
Tensile Properties of Neat Copolymers and PAs

Material	Young's modulus, E (MPa)	Poisson's modulus, μ	Tensile strength, σ_b (MPa)
PA1	3098 ± 30	0.430	38 ± 2
PA2	2767 ± 30	0.430	41 ± 2
mPE1	69 ± 5	0.430	13 ± 2
mPE1-*g*-MA	61 ± 5	0.43	13 ± 2
mPE2-*g*-MA	5.3 ± 0.6	0.470	5.0 ± 0.5
mEPDM	12.0 ± 0.5	0.495	4.0 ± 0.3
mEPDM-*g*-MA	11.0 ± 0.5	0.495	4.0 ± 0.3
EPDM-*g*-MA	7.0 ± 0.6	0.498	5.0 ± 0.4
mEPR-*g*-MA	2.0 ± 0.5	0.493	5.0 ± 0.4

strength of 13 and 5 MPa and different Poisson's modulus are shown in Figure 10. It can be seen that a dispersed phase material with a low Young's modulus and low Poisson's modulus has a high cavitations deformation value when the tensile strength is fixed at 13 MPa. However, low cavitations deformation values were obtained with dispersed phase materials with the highest Poisson's modulus, high Young's modulus, and 5 MPa of tensile strength.

As well, the notched Izod impact values of the binary blends as a function of the cavitations deformation values of the different dispersed phases calculated by the Liang model are presented in Figure 11. The EPDM-*g*-MA sample showed the lowest cavitations deformation value, and the binary blend prepared with this material as dispersed phase has the highest Izod impact strength at room temperature (Fig. 11). The Izod impact strength values at room temperature of the reactive binary blends were in accordance with these cavitations deformation values (see Fig. 11). On the other hand, the interparticle distance effect was explained by Lazzery et al.[39] on the basis of the stabilization effect of dilatational band propagation exerted by stretched rubber particles. Then, the effectiveness of the grafted copolymers as impact modifier depends on the morphology of the blends and a combination of tensile properties of the blend components such as, Young's modulus, Poisson ratio, and break stress of these grafted materials by using the Liang model.[11]

Many authors have stated that dispersed rubberlike particles constitute preferential sites of cavitations due to the contrast of elastic modulus with the matrix. Such particles can be plain elastomer droplets (binary blends) and also core-shell particles (ternary blends) in which the rubber occupies a thin enveloped only. In ternary blends, the shell undergoes cavitations while the core ensures sufficient rigidity. Also, the thickness of the rubber interlayer in ternary blends is affecting the rubber cavitations. In blends with low compatibilizer content and/or compatibilizer with a low grafting degree, the rubber interlayer is thin, and the crack propagates easily across the section.[35–37] The low-notched Izod impact strength obtained in the mPE1/PA1/mEPR-*g*-MA (B10) ternary blend in comparing with the other ternary blends (B8 and B9) can be explained by the

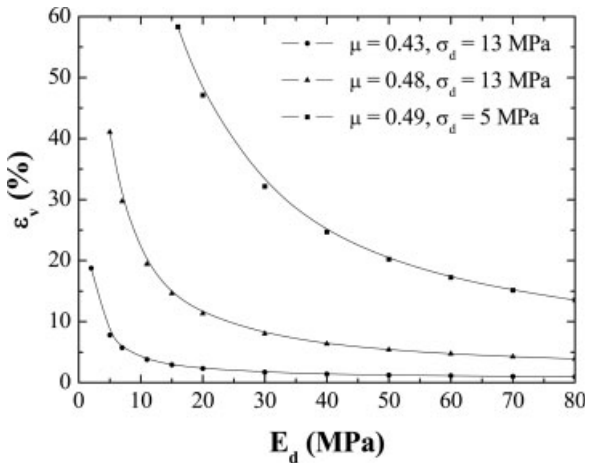

Figure 10 Cavitations deformation values (ε_v) as a function of the Young's modulus of the dispersed phase (E_d) calculated for materials with different Poisson modulus (μ) and stress strength (σ_d).

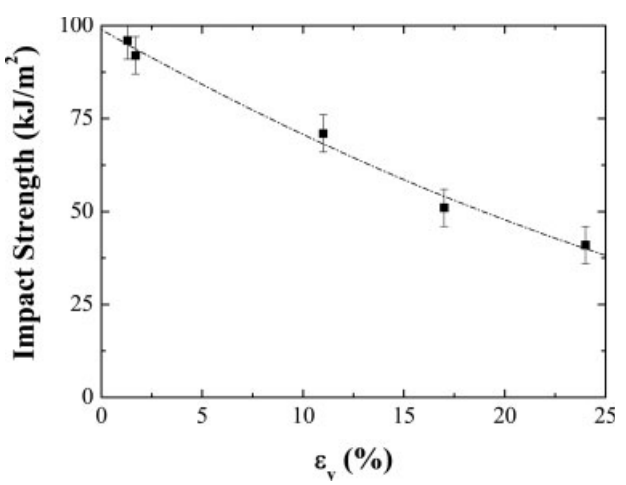

Figure 11 Notched Izod impact strength of the binary blends as a function of the cavitations deformation values of dispersed phase (ε_v).

TABLE VII
Yield Stress (σ_y), Tensile Strength (σ_b), Elongation at Break (ε_b), Puncture Impact Values at 23°C and Vicat Temperature for the PAs and Their Blends

Material or blend	$\sigma_y \pm 2$ (MPa)	$\sigma_b \pm 2$ (MPa)	ε_b (%)	Puncture impact values (J)	Vicat temperature (°C)
PA1	59	38	–	117 ± 2	189 ± 2
PA2	59	41	–	116 ± 2	191 ± 2
B1	57	39	124 ± 16	–	150 ± 2
B2	39	37	56 ± 15	–	134 ± 2
B3	36	38	115 ± 12	76 ± 3	132 ± 6
B4	56	49	134 ± 16	–	171 ± 2
B5	41	42	76 ± 10	–	136 ± 3
B6	41	51	97 ± 15	75 ± 3	157 ± 5
B7	35	39	56 ± 12	–	134 ± 6
B8	37	41	48 ± 12	71 ± 4	132 ± 5
B9	42	36	113 ± 12	85 ± 4	148 ± 5
B10	38	37	86 ± 10	21 ± 6	144 ± 5

higher Young's modulus and lower Poisson modulus of the mPE1 than that of mEPDM that probably increase the modulus of the core-shell mPE1/mEPR-*g*-MA particles.

On the other hand, an additional requirement was needed to obtain blends with high Izod impact strength at −30°C of temperature. The test temperature should be higher than the glass transition temperature (T_g) of the dispersed phase, determined by dynamic mechanical analysis. The storage modulus significantly decreases at this glass transition temperature for amorphous polymers. The glass transition temperature of EPDM rubbers is lower than that of EPR-*g*-MA copolymer (−23°C). Thus, the lowest Izod impact strength of the EPR-*g*-MA/PA binary blend found at −30°C of temperature. For semicrystalline polymers like PEs, there is a gradual reduction in the storage modulus. Then, the lowest impact strength at −30°C of the binary blends prepared with metallocene polythylenes (B2 and B3 blends).

The tensile properties of the neat materials are shown in Table VI. Nonsignificant differences in tensile stress–strain behavior were observed at low strain for the mPE1, mEPDM, and its *in situ* grafted samples. Only a small reduction in Young's modulus was observed. The tensile properties (yield stress, tensile strength, and elongation at break) of the blends are presented in Table VII. The Young's modulus of the PAs and their blends are shown in Figure 12. The significant reduction in Young's modulus (E) values for the binary and ternary reactive PA blends limits the applicability of these materials. This result may be ascribed to the high compatibilization effect of the functionalized dispersed phases and/or grafted commercial compatibilizers.[5–7] As well, the reduction in the yield stress (σ_y) can be explained by a cavity nucleation process presents during the tensile test, possibly due to the stress concentration induced by the dispersed phase particles, by the plastic deformation mechanism that involves significant dilatational strain and/or by lower crystallinity of this dispersed phase.[11,34,36–38] However, the reactive blends based on mEPR-*g*-MA (B6 and B9) showed a greater cold drawing than those based on EPDM-*g*-MA (B7 and B8). Similar results were found by Okada et al.[7] in their blends with the same EPR-*g*-MA material.

On the other hand, the Vicat temperature values of the PAs and their blends can be related to the flexural mechanical properties and the variation of the flexural modulus with the temperature. In our case, the Vicat temperature values of the neat PAs and their blends could be related to the tensile modulus and cold-drawing process at room temperature in binary blends (B1, B4, and B6). So, the high Vicat temperature values obtained for the nonreactives mPE1/PA1 and mEPDM/PA2 and reactive mEPR-*g*-MA/PA2 binary blends.

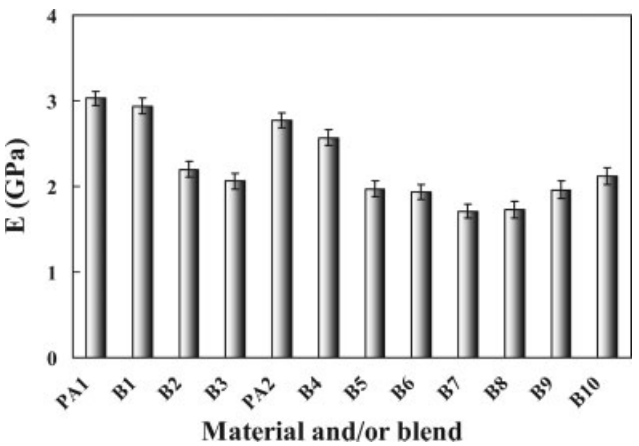

Figure 12 Young's modulus of the PAs and their blends at room temperature.

CONCLUSIONS

The effectiveness of the compatibilization systems studied in this work was confirmed by the increase of the notched Izod impact properties of the binary and ternary blends at room temperature and −30°C of temperature. The reactive blends based on the maleated copolymer with the lowest ethylene crystallinity showed the lowest tensile modulus and yield stress and the highest notched Izod impact strength at room and −23°C of temperatures. The results indicated that the effectiveness of the grafted copolymers as impact modifier depend on the morphology of the blends and a combination of tensile properties of the blend components such as Young's modulus and Poisson ratio and break stress of these grafted materials. The blend with the better combination of mechanical properties was PA2/mEPDM-*g*-MA. High toughness and tensile modulus were obtained for this blend.

References

1. Baker, W.; Scott, C.; Hu, G.-H. Reactive Polymer Blending; Hanser: Munich, 2001.
2. Majumdar, B.; Keskkula, H.; Paul, D. R. J Appl Polym Sci 1994, 54, 339.
3. Huang, J. J.; Keskkula, H.; Paul, D. R. J Polym 2004, 45, 4203.
4. Anttila, U.; Hakala, K.; Helaja, T.; Löfgren, B.; Sépala, J. J Polym Sci Part A: Polym Chem 1999, 37, 3099.
5. Yu, Z.-Z.; Ou, Y.-C.; Hu, G.-H. J Appl Polym Sci 1998, 69, 1711.
6. Yu, Z.-Z.; Ou, Y.-C.; Qi, Z.-N.; Hu, G.-H. J Polym Sci Part B: Polym Phys 1998, 36, 1987.
7. Okada, O.; Keskkula, H.; Paul, D. R. Polymer 2001, 42, 8715.
8. Margolina, A.; Wu, S. Polymer 1988, 29, 2170.
9. Wu, S. Polymer 1985, 26, 855.
10. Aróstegui, A.; Gaztelumendi, M.; Nazábal, J. Polymer 2001, 42, 9565.
11. Liang, H.; Jiang, W.; Zhang, J.; Jiang, B. J Appl Polym Sci 1996, 59, 505.
12. Wu, S. Polym Eng Sci 1987, 27, 335.
13. Sundararaj, U.; Macosko, C. W. Macromolecules 1995, 28, 2647.
14. Thomas, S.; Groeninckx, G. Polymer 1999, 40, 5799.
15. Premphet, K.; Chalearmthitipa, S. Polym Eng Sci 2001, 4, 11.
16. López-Quintana, S.; Villarreal, N.; Rosales, C.; Gobernado-Mitre, I.; Merino, J. C.; Pastor, J. M. Poster contribution 572, Guimaraes PPS-18, 2002.
17. Oostenbrink, A. J.; Gaymans, R. J. Polymer 1992, 33, 3086.
18. Moad, G. Prog Polym Sci 1999, 24, 81.
19. Samay, G.; Nagy, T.; White, J. J Appl Polym Sci 1995, 56, 1423.
20. Molau, G. E. J Polym Sci 1965, A-3, 4235.
21. Sánchez, A.; Rosales, C.; Laredo, E.; Müller, A. J.; Pracella, M.; Macromol Chem Phys 2001, 202, 2461.
22. Coltelli, M. B.; Passaglia, E.; Ciardelli, F. Polymer 2006, 47, 85.
23. Aguilar, M.; Vega, J. F.; Sanz, E.; Martinez-Salazar, J. Polymer 2001, 42, 9713.
24. Dias, M. L.; Barbi, V.; Pereira, V.; Mano, E. B. Mater Res Innovat 2001, 4, 82.
25. Greco, R.; Musto, P.; Riva, F. J Appl Polym Sci 1989, 37, 789.
26. Wunderlich, B. Thermal Analysis; Academic Press: New York, 1990.
27. Jiang, C.; Filippi, S.; Magagnini, P. Polymer 2003, 44, 2411.
28. Huang, J. J.; Keskkula, H.; Paul, D. R. Polymer 2006, 47, 624.
29. Huang, J. J.; Keskkula, H.; Paul, D. R. Polymer 2006, 47, 639.
30. Huang, J. J.; Keskkula, H.; Paul, D. R. Polymer 2006, 47, 3505.
31. Do, C. H.; Pearce, M.; Bulkin, B. J. J Polym Sci Part A: Polym Chem 1987, 25, 2409.
32. Scaffaro, R.; La Mantia, F. P.; Canfora, L.; Polacco, G.; Filippi, S.; Magagnini, P. Polymer 2003, 44, 6951.
33. Jurkowski, B.; Kelar, K.; Ciesielska, D. J Appl Polym Sci 1998, 69, 719.
34. Dean, G.; Read, B. Polym Test 2001, 20, 677.
35. Bai, S. L.; Wang, G. T.; Hiver, J. M.; G'Sell, C. Polymer 2004, 45, 3063.
36. G'Sell, C.; Bai, S. L.; Hiver, J. M. Polymer 2004, 45, 5785.
37. Bai, S. L.; G'Sell, C.; Hiver, J. M.; Mathieu, C. Polymer 2005, 46, 6437.
38. Wu, S. J Appl Polym Sci 1988, 35, 549.
39. Lazzeri, A.; Thio, Y. S.; Cohen, R. E. J Appl Polym Sci 2004, 91, 925.